X-ray studies of aligned magnetic stripe domains in perpendicular multilayers

O. Hellwig,[1] G. P. Denbeaux,[2] J. B. Kortright,[2] and Eric E. Fullerton[1]

[1]*San Jose Research Center*
Hitachi Global Storage Technologies
650 Harry Road, San Jose, CA 95120, USA

[2]*Materials Science Division*
Lawrence Berkeley National Laboratory
Berkeley, CA 94720, USA

We have investigated the stripe domain structure and the magnetic reversal of perpendicular Co/Pt based multilayers at room temperature using magnetometry, magnetic imaging and magnetic x-ray scattering. In-plane field cycling aligns the stripe domains along the field direction. In magnetic x-ray scattering the parallel stripe domains act as a magnetic grating resulting in observed Bragg reflections up to 5th order. We model the scattering profile to extract and quantify the domain as well as domain wall widths. Applying fields up to ~1.2 kOe perpendicular to the film reversibly changes the relative width of up versus down domains while maintaining the overall stripe periodicity. Fields above 1.2 kOe introduce irreversible changes into the domain structure by contracting and finally annihilating individual stripe domains. We compare the current results with modeling and previous measurements of films with perpendicular anisotropy.

Keywords: magnetic domains, perpendicular magnetic anisotropy, x-ray scattering, magnetic microscopy, magnetic thin films

Introduction

Magnetic thin films with perpendicular magnetic anisotropy (*e.g*. Co/Pt multilayers) often form stripe domains to lower the magnetostatic energy [1-4]. The width of these domains is determined by the balance between magnetostatic versus domain wall energies and varies with film thickness. The morphology of the domains depends on the field history. Demagnetizing the films with a perpendicular applied field results in labyrinth stripe domains with random in-plane orientation. However, demagnetizing the film with an in-plane magnetic field couples to the in-plane magnetization component of the domain wall and aligns the stripe domains parallel to the external field direction.

We use resonant magnetic X-ray scattering and imaging techniques to study the evolution of aligned magnetic stripe domains in perpendicular Co/Pt based multilayers. Both techniques detect transmitted photons and obtain magnetic contrast from the resonant magnetic term in the atomic scattering factor that is first order in the magnetization [5,6]. A photon based imaging X-ray microscope (XRM) exploits X-ray Magnetic Circular Dichroism (XMCD) as the contrast mechanism [7, 8]. XRM is an excellent tool for such studies because the photon-in-photon-out technique does not perturb the sample during measurement and is insensitive to applied fields as compared to magnetic force microscopy (MFM). This is especially important for studying domain nucleation and annihilation processes in an external magnetic field. Resonant magnetic small-angle scattering complements the imaging studies and provides ensemble-averaged domain structure and reversal properties [6]. Combining real and reciprocal space techniques we obtain information about both the specific behavior of individual domains when nucleating and propagating as well as the ensemble averaged microscopic properties of the system such as stripe periodicity, stripe correlation length, and domain wall width.

Experimental procedures

The perpendicular films used for our experiments are CoO(10Å){[Co(4Å)/Pt(7Å)]$_4$ Co(6Å)CoO(10Å)}$_{10}$ multilayers originally deposited for low temperature exchange bias studies that have been reported elsewhere [9]. In the current study the films are investigated at room temperature. Since this is above the CoO Néel temperature the films behave as simple perpendicular anisotropy films since the CoO layers just acts as non-magnetic spacers [9]. The multilayers were deposited onto Si_3N_x-coated Si substrates and Si_3N_x-membranes to facilitate transmission x-ray measurements. They were grown onto a 200-Å Pt underlayer by DC magnetron sputtering at ambient temperatures. A 20-Å Pt cap layer protects the multilayer from any further oxidation after preparation. The perpendicular easy axis in the system is obtained via the high surface anisotropy of the 4-Å Co layers. The Pt buffer layer and the multilayer are (111) textured with a mosaicity of ~10º. A more detailed description of the samples is given in Ref. 9.

The macroscopic magnetic properties were characterized using polar magneto-optical Kerr effect (MOKE) and SQUID magnetometer. Remanent domain images were obtained by MFM. Transmission x-ray microscopy (XRM) was used to probe the domain structure in applied fields up to 3.4 kOe during reversal [7, 8]. The field dependence of the domain structures was also characterized via resonant soft x-ray magnetic small-angle scattering (SAS) [5, 9, 10]. X-ray measurements were performed at the Advanced Light Source (ALS) at the Lawrence Berkeley National Laboratory on undulator beamlines 4 and 8 for SAS and using the XM1 zone-plate imaging microscope on bending magnet beamline 6.1.2 for x-ray magnetic imaging. In both cases, we used magnetic films deposited onto silicon nitride membranes that

were measured in transmission geometry. To enhance the magnetic contrast we tuned the energy to the Co L_3 absorption edge (~ 778 eV, ~ 1.59 nm). For the SAS analysis we performed θ–2θ scans with an apertured diode detector using linear polarization, while the XRM imaging was done with a 2-dimensional CCD camera using elliptical polarization from above the synchrotron orbit plane.

Results and discussion

The magnetic reversal of our films is characterized by domain nucleation, propagation, and annihilation as indicated on the hysteresis loop shown in Fig.1. The high magnetostatic energy in the uniformly magnetized state is reduced via up and down stripe domains where the characteristic width, w, of the periodic or quasi-periodic domains varies with total film thickness, t. Increasing t from the ultra thin limit usually leads to an exponential decrease of the domain size followed by a slow increase that scales as $\sqrt{t}$ [1-3]. The domain morphology depends sensitively on the field history. In remanence after out-of-plane saturation the multilayers exhibit a labyrinth domain pattern as shown in the MFM image of the $[(Co/Pt)_4Co/CoO]_{10}$ multilayer in Fig.2a. The dark and light contrast represents domains with magnetization pointing out of and into the plane of the film, respectively. The average domain width determined from the MFM image is ≅ 130 nm. Applying a saturating in-plane magnetic field with subsequent in-plane AC demagnetization significantly alters the domain pattern. The domains exhibit a preferred alignment along the applied field direction and form parallel stripe domains as shown in Fig. 2b. In the aligned case the average domain width is reduced and we obtain a value of ≅ 90 nm.

Fig.2c shows the resonant magnetic SAS scans from a similarly prepared multilayer on a membrane in both the labyrinth (solid symbols) and the aligned state (open symbols) together

with a theoretical fit for the aligned state (solid line). The scattering from the labyrinth sample is similar to that observed in Ref. 6. We observe a broad maximum at q = 0.024 nm^{-1} that corresponds to an average domain periodicity of $2\pi/q$ = 260 nm, the average periodicity of an up-down domain pair. The intensity is equally scattered in all in-plane directions resulting in an isotropic donut-like intensity distribution in 2-dimensional reciprocal space [10]. The magnetic structure has only limited long-range order and resembles the scattering from a static liquid. From the width Δq = 0.0173 nm^{-1} of the peak we estimate an in-plane correlation length of $2\pi/\Delta q \cong$ 360 nm.

In contrast, the aligned stripe domain pattern can be considered as a 1-dimensional magnetic grating, which results in an anisotropic SAS. We orient the sample with the scattering vector $\boldsymbol{q}$ in-plane and perpendicular to the domains in order to probe the magnetic structure. In that case a radial q scan exhibits a diffraction pattern with well-defined Bragg peaks corresponding to the domain periodicity [11,12]. Due to the symmetry of the domain pattern, the Bragg reflections are only observed in the direction perpendicular to the stripes leading to a significant intensity increase in the radial profiles through reciprocal space. The first, third and fifth order reflections are observed. Even-order reflections are suppressed because up and down domains have equal width at remanence. Compared to the random domains the first order peak position is shifted to higher q values, which can be accounted for by reduction of the characteristic domain width from $\cong$ 130 nm down to $\cong$ 90 nm with alignment, consistent with the MFM findings. The width of the first peak narrows significantly compared to the labyrinth case, yielding a correlation length $\cong$ 970 nm. This narrowing is consistent with the increased intensity of higher orders for the aligned case.

The solid line through the measured SAS data for the aligned stripes in Fig.2c is a fit of the data to the domain profile shown in the inset using a model developed in the Appendix. For simplicity, we assumed a linear domain wall profile with thickness t_{DW}. In addition to the average profile we also assumed cumulative Gaussian fluctuations in the domain size to account for the disorder present in the image and the broadening of the higher order diffraction peaks. The fitting parameters were the domain periodicity, the domain wall width and the root mean square of the domain size fluctuations. We obtained a value of 90 nm for the domain width w with a root-mean-square fluctuation of 9 nm about the average domain width, and 25 nm for the domain wall width.

Figures 3a and 3b show the evolution of the SAS of the stripe domain pattern from remanence to saturation with the external field applied out-of-plane along the easy axis. Corresponding XRM images from a similar $[Co/Pt]_{50}$ multilayer are shown in Fig. 3c and 3d. The stripe pattern is found to be completely reversible below applied fields of ~1.2 kOe, *i.e.,* when the field is removed the original alignment is regained. The reversible part of the field evolution from remanence to about 1.2 kOe is shown in Fig.3a, while the irreversible switching above 1.2 kOe is plotted in Fig.3b. In the reversible part one domain grows at the expense of the other and the intensity of each harmonic changes with field (Fig. 3a). While the first order reflection decreases only slightly with increasing fields, the intensity of the higher order reflections have much stronger field dependencies. The intensity of the second and fourth order reflections, suppressed at remanence, monotonically increase with field, while the intensity of the third order reflection monotonically decreases to zero as the field increases.

Applying out-of-plane fields > 1.2 kOe introduces irreversible magnetization changes and the well-defined stripe domain diffraction pattern slowly disappears. This is shown in reciprocal

space in Fig. 3b and in real space Fig. 3c. We observe in reciprocal space a superposition of the well-defined harmonics together with an intensity increase towards low q values due to the introduced disorder in the domain structure. The period of the remaining ordered stripe phase is the same as that observed at remanence as the relative intensity of the ordered phase decreases towards saturation. This behavior is different from Kooy and Enz's classic study of $BaFe_{12}O_9$ [2], where the change in the overall periodicity is the fundamental saturation mechanism. They observe that the stripe periodicity diverges as saturation is approached [2]. Instead, we observe that specific stripe domains are irreversibly deleted from the magnetic grating when applying fields > 1.2 kOe. This annihilation process introduces disorder into the system that does not appear to be completely random. Weak diffraction peaks are observed at the expected ½ order and $\frac{3}{2}$ order positions in an applied field of 1.92 kOe. This suggests that as stripes disappear from the system, they do so in a way that leads to some period doubling of the magnetic structure, *i.e.*, it is more likely that every other stripe domain is deleted rather than neighboring stripe domains. This tendency can also be observed in the XRM image in Fig. 3c taken at 1.6 kOe.

Returning to remanence from fields between 1.2 and 2 kOe creates regions of labyrinth domains where some stripe domains were deleted from the system. This is demonstrated in Fig.4. in a minor loop between remanence and –1.6 kOe. Image (a) shows the as-prepared stripe state, (b) is the same spot at –1.6 kOe and (c) shows the domain structure after returning to remanence. The straight stripe domains that were annihilated at -1.6 kOe return with a significant degree of disorder. Even the well-defined environment of ordered stripe domains does not prevent the introduction of defects into the domains that return as the applied field is removed. It is apparent that the annihilation of individual domains is a non-reversible process.

Applying even higher fields > 2 kOe destroys the alignment completely and the broad intensity distribution at low q dominates the scattering profile (Fig. 3b), indicating that saturation is reached via uncorrelated magnetic regions seen as isolated stripes in Fig. 3c for a field of 2.2 kOe. With increasing field, the stripe domains first reduce their width significantly before they are annihilated or contracted down to a zero-dimensional spot like domain.

Upon saturation the SAS intensity drops to zero confirming that we are observing only magnetic scattering from our samples in the q range of interest. The return to remanence after applying a saturating field is shown in Fig. 3d in a sequence of XRM images. Reverse domains are nucleated in the film and then grow with decreasing field. The nucleation typically proceeds from a few zero-dimensional (spot-like) domains that first increase in diameter up to a critical size before they expand out into one-dimensional stripe domains. What appears as the nucleation field corresponds to the avalanche-like expansion of these labyrinth stripe domains [13]. The domains that evolve from each nucleation site coalesce towards remanence by forming the labyrinth domain pattern (Fig. 3d) shown before in Fig. 2a. A similar process is described in Refs 1 and 2.

In Fig. 5 we summarize the results (of Figs. 3a and 3b) by plotting the intensity development of the different harmonics (1^{st} – 4^{th}) versus externally applied field of both the experimental SAS data (open symbols) and the theoretical profiles (solid symbols). There is a suppression of the even orders in remanence and a suppression of the third order at ~1.1 kOe, indicating that a domain width ratio of 2:1 is present at that field. The peak positions of the different harmonics stay fixed with applied field. This indicates that the overall periodicity of the stripe pattern remains constant while the width ratio of up versus down domains changes reversibly from 1:1 at 0 Oe to 1:2 at 1.1 kOe.

The calculated intensities in Fig. 5 assume completely reversible behavior with no topological changes in the domain structure. The domain wall width, periodicity and disorder were determined from the fit shown in Fig. 2 and assumed constant with applied field. The ratio of the up and down domains was then assumed to vary linearly with field constant with linear low field response of the magnetization. The good agreement between theory and experiment thus suggests that reversible changes and linear dependence on field dominate the reversal up to about 1.2 kOe. For higher fields this model no longer holds.

Another indication for that conclusion is provided by plotting the experimental intensity development at the lowest q value accessible (q = 0.015 nm^{-1}, 420 nm periodicity) as shown by the open diamonds in Fig. 5. From its intensity evolution it can be inferred that uncorrelated magnetic structure with broad low q intensity dominates the nucleation and saturation processes, while a characteristic magnetic length scale governs domain wall propagation near remanence. As a result the intensity observed at very low q, which serves as a measure of disorder and non correlation in the domain structure, exhibits a sharp increase at an applied field of ~1.3 kOe.

Both imaging and scattering consistently show that the Co/Pt multilayers and Co/Pt multilayers interleaved with CoO at room temperature are behaving as expected for a thin film with perpendicular anisotropy. The overall results are similar to those observed in a variety of studies of stripe domains in thin films [1-4]. However, as mentioned above, we also observe some significant differences.

Even though different perpendicular thin film systems exhibit very similar remanent stripe domain states, the evolution of such domains with increasing perpendicular field can vary significantly. Annihilation of stripe domains can occur in various ways depending on their mobility. Kooy and Enz [2] have shown that in 3-μm thick $BaFe_{12}O_9$ plates, saturation is

reached by changes in both the stripe domain periodicity and the relative width of up versus down domains such that the domain periodicity diverges towards saturation and stripes are annihilated by being expelled from the sample edge. The domain system as a whole, rather than individual stripe domains, responds to the externally applied field. In our system the saturation behavior is very different. Although we also observe a change in the relative width of up versus down domains, the overall periodicity of the stripe domains remains constant. We do not observe any synchronized expansion of the domain periodicity. Instead, beyond a certain critical field (~1.2 kOe), domains start to annihilate independently without influencing or shifting any of the surrounding domains. Individual stripe domains break along their length, shrink in length, and finally contract down to zero-dimensional spots before being completely annihilated.

Obviously in the Kooy and Enz case, domains and domain walls can easily move through the film. Evidently this is not true for our samples. Although the low coercive field and the ability to align the domains into parallel stripes reflect a certain amount of domain mobility, the saturation process is very different. One possible reason for this different behavior might involve the finite domain walls widths. Since the dimensions of our domains are roughly an order of magnitude smaller than those observed by Kooy and Enz, they have roughly 10 times the number of domain walls per area in the aligned stripe case. Since the moments and anisotropies are similar in the two different samples, the domain wall widths are expected to be similar. As a result, the areal fraction occupied by domain walls is much larger and thus it may become more difficult to move domains in the synchronized way as modeled and observed in the Kooy and Enz study. Another possible reason for the different saturation behavior might be a higher defect density present in our films. From the real space images it is apparent that our stripe patterns are less smooth than those observed in Kooy and Enz. The origin of this domain

roughness may be local roughness variations in the multilayer or grain boundary defects that do not prevent alignment of the domains, but might be strong enough (together with the increased domain wall density) to prevent a synchronized response of the domains towards saturation.

Conclusion

In summary, we have used resonant x-ray scattering as well as x-ray microscopy to study the field evolution of aligned stripe domains in films with perpendicular anisotropy. The scattering results are quantitatively modeled to give ensemble average information regarding the relative size of up and down domains, domain wall thickness, and domain fluctuations. Scattering clearly reveals two distinct regimes. At low fields there is a reversible change in the relative up to down domains with no significant change in the stripe domain morphology. At higher field there is irreversible domain annihilation that leads to significant disorder of the domain structure. The real space images are consistent with interpretation of scattering results, and are especially useful by providing detailed information about domain behavior in disordered regions of the sample. The real and reciprocal space techniques are clearly complementary, and together provide more information than either separately. While the observed reversal behavior has some commonality to previous studies of similar stripe domain systems, we also observe distinct differences. Differences in domain sizes and the influence of thin film microstructure in different systems are suggested as causes for the observed differences.

Appendix

For magnetic scattering in a transmission geometry the scattering cross section is, to first order, proportion to the z (normal to the film) component of the magnetization [6]. Thus the expected scattering intensity $S(q_x)$ in the kinematic approximation for stripe domains with a periodicity Λ is given by

$$S(q_x) = |F|^2 \frac{1 - \exp(iq_x N\Lambda)}{1 - \exp(iq_x \Lambda)} \tag{A1}$$

where q_x is the scattering wavevector in the film plane, N is the number of stripes that scatter coherently, and F is the scattering amplitude for a single period (an up and down domain) given by:

$$F = \int_0^{\Lambda} M_z(x) \exp(iq_x x)\, dx \tag{A2}$$

This model assumes that the domains are periodic and are reproduced exactly. To incorporate fluctuations in the domain periodicity seen in the images and reflected in the broadened higher order diffraction peaks, one needs to incorporate disorder in the model. This is often done based on the approach of Hendricks and Teller [13] that treats disorder as a random sequencing of layers where either the scattering power of the layers or the relative phase between layers varies randomly as one moves through the structure. To include these effects the integrated scattering intensity $S^{int}(q_x)$ is given by ensemble averaging the intensity of all the possible sequences of different layer thicknesses:

$$S^{int}(q_x) = \left\langle \left| \sum_{\mathbf{n}}^{N} F_n \exp\left(i q_x \sum^{n-1} \Lambda_n \right) \right|^2 \right\rangle \tag{A3}$$

where F_n and Λ_n are the structure factor and domain period of the n^{th} period, respectively. Both the scattering amplitude F_n and period Λ_n is allowed to vary from period to period and the brackets < > represent the ensemble average over all possible sequences. A closed form expression for Eq. A3 can be written under the assumption that fluctuations from the average domain structure are cumulative (i.e. a phase error in one layer perturbs all subsequent layers) but are statistically independent for each layer. Under these assumptions it can be shown that Eq. (A3) reduces to [14-16]:

$$S^{int}(q_z) = N\langle F * F\rangle + 2\,\mathrm{Re}\left[\langle F\rangle \Phi\Psi / T\right] \tag{A4}$$

where Re refers to the real component within the brackets and $\langle F\rangle$ and $\langle F^*F\rangle$ are the ensemble average over all possible scattering amplitudes and intensities from individual domain periods, respectively. The remaining terms are given by:

$$T = \left\langle \exp\left(i q_x \Lambda\right)\right\rangle,\ \Phi = \left\langle \exp\left(i q_x \Lambda\right) F^*\right\rangle,\ \Psi = \frac{N - (N+1)T + T^{N+1}}{(1-T)^2} - N \tag{A5}$$

where the brackets in T and Φ ensemble average over all possible periods. These terms relate the scattering interference from different domains.

These expression can be made explicit for the unit cell of an up-down domain pair that can be described with a scattering factor F_A and F_B and domain widths w_A and w_B, respectively. The ensemble averaged parameters become:

$$\begin{aligned}
&\langle F\rangle = \langle F_A\rangle + T_A\langle F_B\rangle \\
&\langle F^*F\rangle = \langle F_A{}^*F_A\rangle + \langle F_B{}^*F_B\rangle + 2\mathrm{Re}\left[\Phi_A\langle F_B\rangle\right] \\
&\Phi = T_B\Phi_A + \Phi_B \\
&T = T_A T_B
\end{aligned} \tag{A6}$$

where fluctuations are averaged over the individual up and down domains A and B where $\Phi_A = \langle \exp(i q_z w_A) F_A{}^* \rangle$ and $T_A = \langle \exp(i q_z w_A) \rangle$ with similar terms for layer B.

For the domain profile shown in the inset of Fig. 3 with a linear domain wall of width *d* and domain widths w_A and w_B for the down and up domains respectively, the scattering amplitude for one domain F_A is given by

$$\begin{aligned}
F_A(q_x) &= \int_0^d \left(-M + \frac{2Mx}{d} \right) \exp(iq_x x)\,dx + \int_d^{w_A} M \exp(iq_x x)\,dx \\
&= \left(\frac{2M}{d\,q_x^2} \right)\left(\exp(iq_x w_A) - 1\right) - \left(\frac{iM}{q_x} \right)\left(\exp(iq_x w_A) + 1\right)
\end{aligned} \tag{A7}$$

There is a similar equation for F_B obtained by changing the sign of M and replacing w_A with w_B.

To incorporate the role of disorder we assume that the domain sizes vary randomly by a Gaussian distribution about the average with width σ. Under this assumption $\langle F_A \rangle$ is given by:

$$\begin{aligned}
\langle F_A\rangle &= \int_{-\infty}^{\infty} F_A(t_A + \Delta) \frac{1}{\sigma\sqrt{2\pi}} \exp\left(-\tfrac{1}{2}(\Delta/\sigma)^2\right) d\Delta \\
&= \left(\frac{2M}{d\,q_x^2} \right)\left(\exp(iq_x t_A) - 1\right) - \left(\frac{iM}{q_x} \right)\left(\exp\left(iq_x t_A - \tfrac{1}{2}\sigma^2 q_x^2\right) + 1\right)
\end{aligned} \tag{A8}$$

Similar expressions can be derived for the remaining terms in Eq. (A6) and are given by

$$\left\langle F_A F_A^* \right\rangle = \left(\frac{8M^2}{d^2 q_x^4}\right)\left[1-\cos(q_x d)\right] + \left(\frac{2M^2}{q_x^2}\right)\left(1+\exp\left(-\tfrac{1}{2}\sigma^2 q_x^2\right)\cos(q_x w_A)\right)$$
$$+\left(\frac{4M^2}{d\, q_x^3}\right)\left[\sin(q_x d)+\exp\left(-\tfrac{1}{2}\sigma^2 q_x^2\right)\left(\sin(q_x w_A)-\sin(q_x (w_A - d))\right)\right], \quad \text{(A9)}$$

$$T_A = \exp\left(-\tfrac{1}{2}\sigma^2 q_x^2 + i q\, w_A\right), \quad \text{(A10)}$$

$$\Phi_A = \left[\left(\frac{2M}{d\, q_x^2}\right)\left(\exp(-iqd)-1\right)+\frac{iM}{q_x}\right]\exp\left(-\tfrac{1}{2}\sigma^2 q_x^2 + i\, q_x\, w_A\right)+\frac{iM}{q_x}. \quad \text{(A11)}$$

The corresponding equation can be derived for domain B by changing the sign of M and replacing w_A with w_B in Eqs. A8 – A11. These expressions can then be substituted into Eq. A4 to obtain the final scattering intensity.

References

[1] C. Kittel, Phys. Rev. **70**, 965 (1946); Rev. Mod. Phys. **21**, 541 (1949).

[2] C. Kooy and U. Enz, Philips Res. Repts. **15**, 7 (1960).

[3] A. Hubert and R. Schäfer, *Magnetic Domains* (Springer-Verlag, Berlin, 1998) Chaps. 3 and 5, and reference within.

[4] A.W. Rushforth, P. C. Main, B.L. Gallagher, C. H. Marrows, B. J. Hickey, E.D. Dahlberg and P. Earnes, Journal of Appl. Phys. **89**, 7534 (2001).

[5] J. B. Kortright and S.-K. Kim, Phys. Rev. B **62**, 12216 (2000).

[6] J. B. Kortright, S.-K. Kim, G. P. Denbeaux, G. Zeltzer, K. Takano, and Eric E. Fullerton, Phys. Rev. B **64**, 092401 (2001).

[7] J. B. Kortright, D. D. Awschalom, J. Stöhr, S. D. Bader, Y. U. Idzerda, S. S. P. Parkin, I. K. Schuller, and H.-C. Siegmann, J. Magn. and Magn. Mater. **207**, 7 (1999).

[8] P. Fischer, G. Denbeaux, T. Eimüller, D. Goll, and G. Schütz, IEEE Trans. Mag. **38**, 2427 (2002).

[9] O. Hellwig, S. Maat, J. B. Kortright, and E. E. Fullerton, Phys. Rev B **65,** 144418 (2002).

[10] B. Hu, P. Geissbuhler, L. Sorensen, S. D. Kevan, J. B. Kortright, and E E. Fullerton, Synch. Rad. News 14, 11 (2001).

[11] H. A. Dürr, E. Dudzik, S. S. Dhesi, J. B. Goedkoop, G. van der Laan, M. Belakhovsky, C. Mocuta, A. Marty, and Y. Samson, Science **284**, 2166 (1999).

[12] G. van der Laan, E. Dudzik, S. P. Collins, S. S. Dhesi, H. A. Durr, M. Belakhovsky, K. Chesnel, A. Marty, Y. Samson, and B. Gilles, Physica B **283,** 171 (2000).

[13] S. Hendricks and E. Teller, J. Chem. Phys. **10**, 147 (1942).

[14] J. Kakinoki and Y. Komura, J. Phys. Soc. Jpn. **7**, 30 (1952).

[15] E. E. Fullerton, Ivan K. Schuller, H. Vanderstraeten, Y. Bruynseraede, Phys. Rev. B **45**, 9292 (1992).

[16] N. Nakayama, T. Okuyama and T. Shinjo, J. Phys.: Condens. Matter **5**, 1173 (1993).

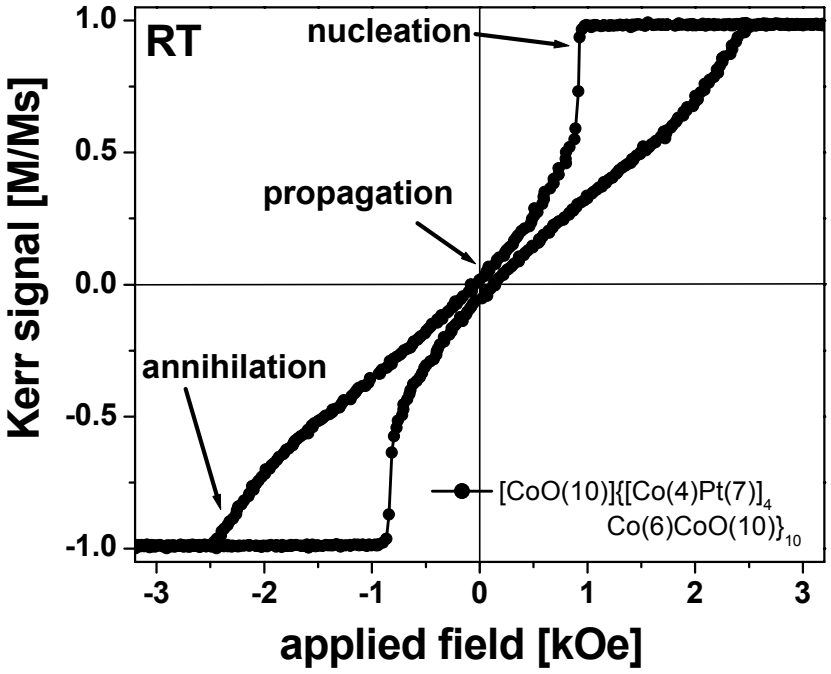

Figure 1: Room-temperature polar MOKE measurements of a $CoO[(Co/Pt)_4Co/CoO]_{10}$ multilayer. The reversal is dominated by domain nucleation, propagation and annihilation.

Figure 1

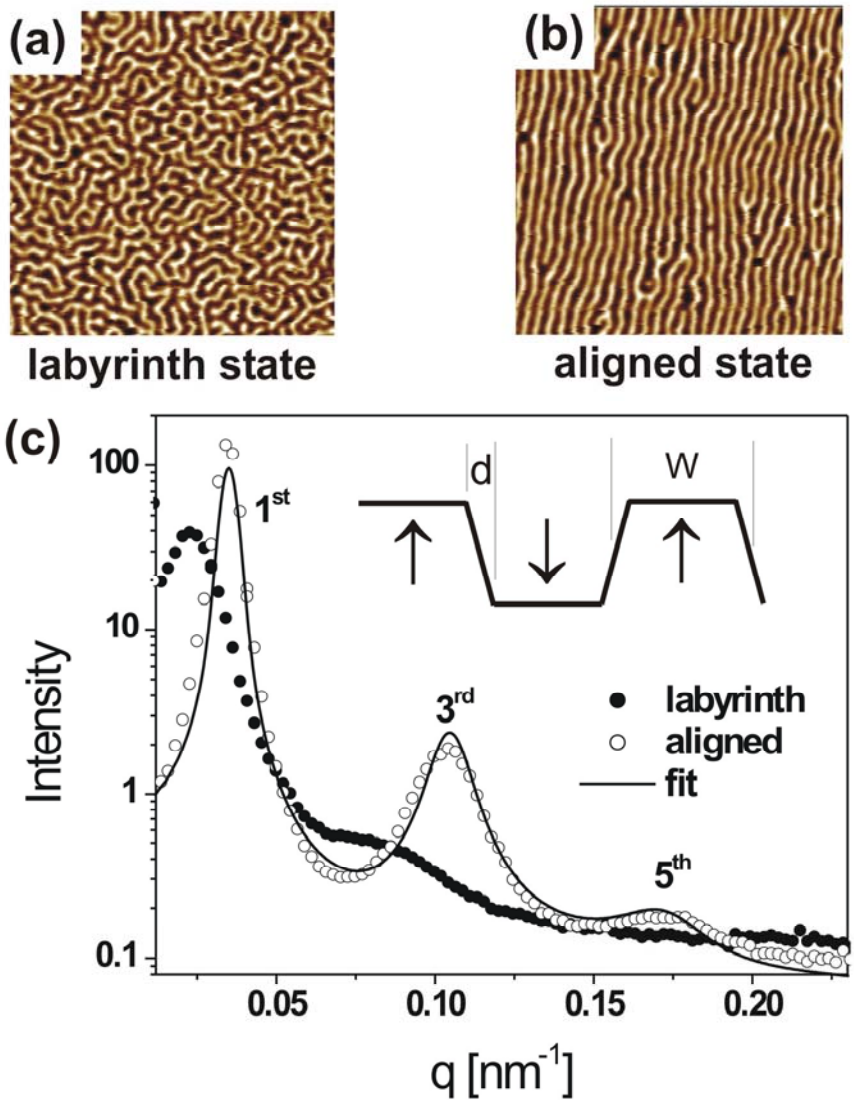

Figure 2: (a) MFM image of the labyrinth domain state after out-of-plane saturation. (b) MFM image of the aligned stripe domain state after in-plane demagnetization along the vertical axis of the image. Each image is $(5\ \mu m)^2$ in size. (c) Corresponding magnetic soft X-ray small angle scattering spectra from the two magnetic domain configurations shown in (a) and (b). For the anisotropic domain structure (b) the incoming X-ray beam was oriented horizontally in order to probe the stripe periodicity. Open symbols show 1^{st}, 3^{rd} and 5^{th} harmonics of the aligned stripes. In the labyrinth state (solid symbols) we only observe 1^{st} and 3^{rd} order due to the increased disorder. The solid line is a theoretical fit to the aligned domain state which allows to extract the one dimensional real space profile i.e. domain width, w, as well as domain wall width, d, as illustrated in the inset.

Figure 2

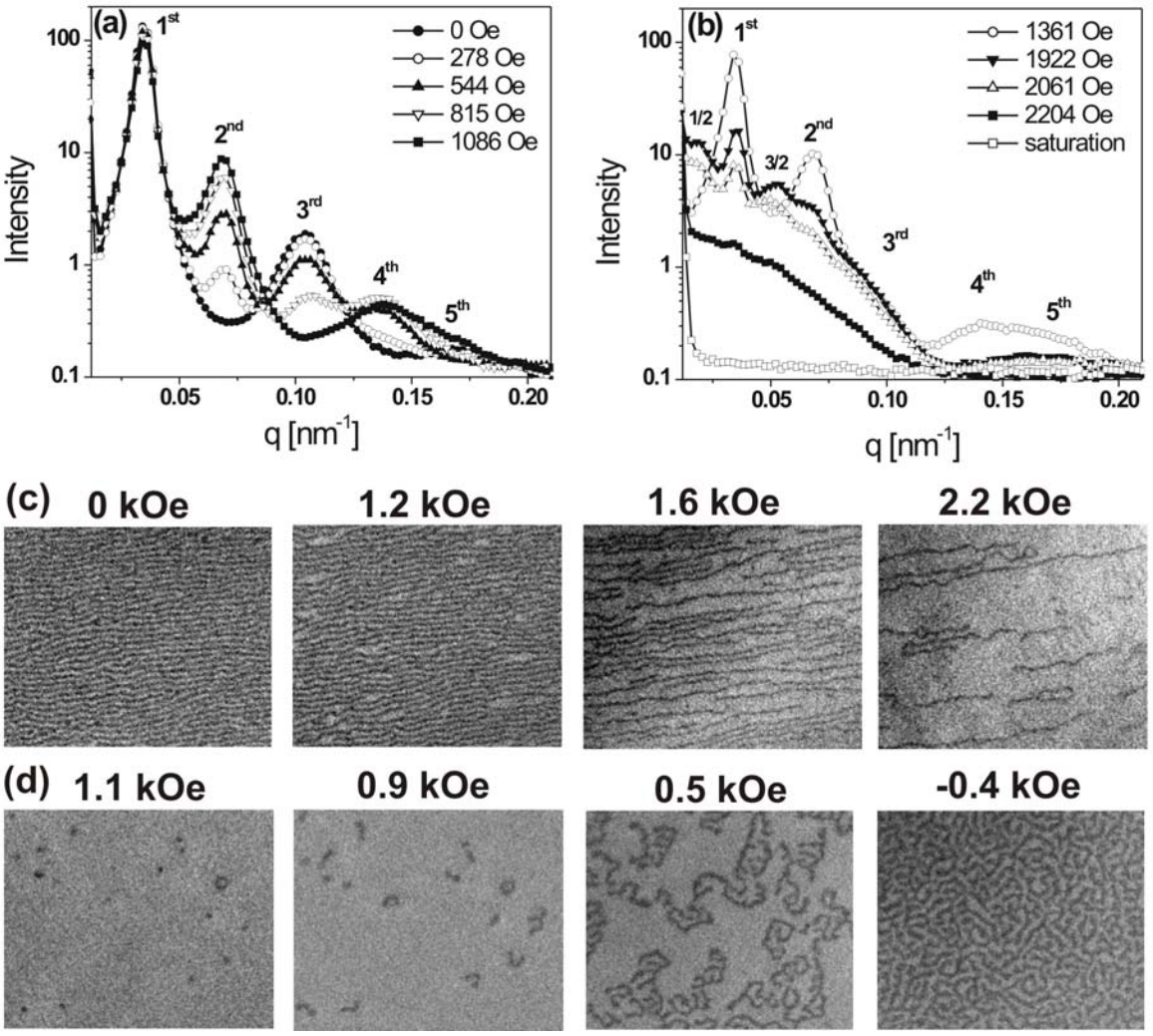

Figure 3: (a) Magnetic small angle scattering spectra of the aligned stripe domain structure with increasing externally applied field from 0 to 1086 Oe at RT (reversible part). (b) Small angle scattering spectra of the stripe domain structure while increasing the externally applied field from 1361 Oe up to saturation at RT (irreversible part). (c,d) X-ray transmission microscopy images of the aligned stripe state going from remanence into saturation (c) and back to remanence (d). Once saturated the sample has no memory of the stripe alignment at RT. Thus back in remanence it ends up in the labyrinth state (as shown in Fig 2a).

Figure 3

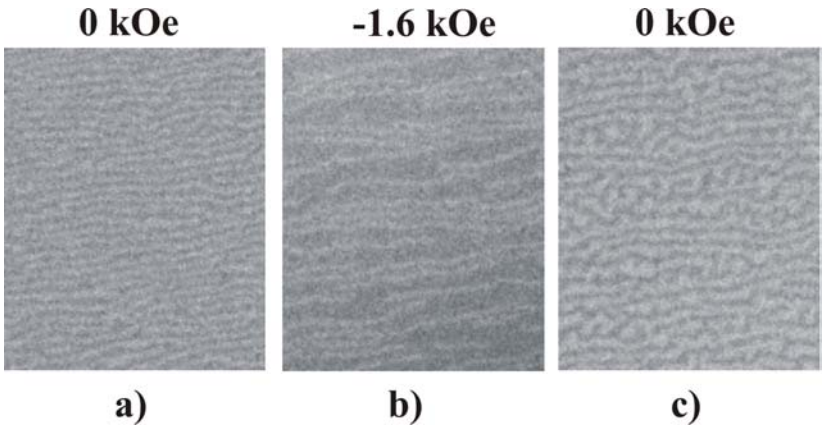

Figure 4: X-ray transmission microscopy images of the aligned stripe state going from remanence (a) to –1.6 kOe (b) and back to remanence (c).

Figure 4

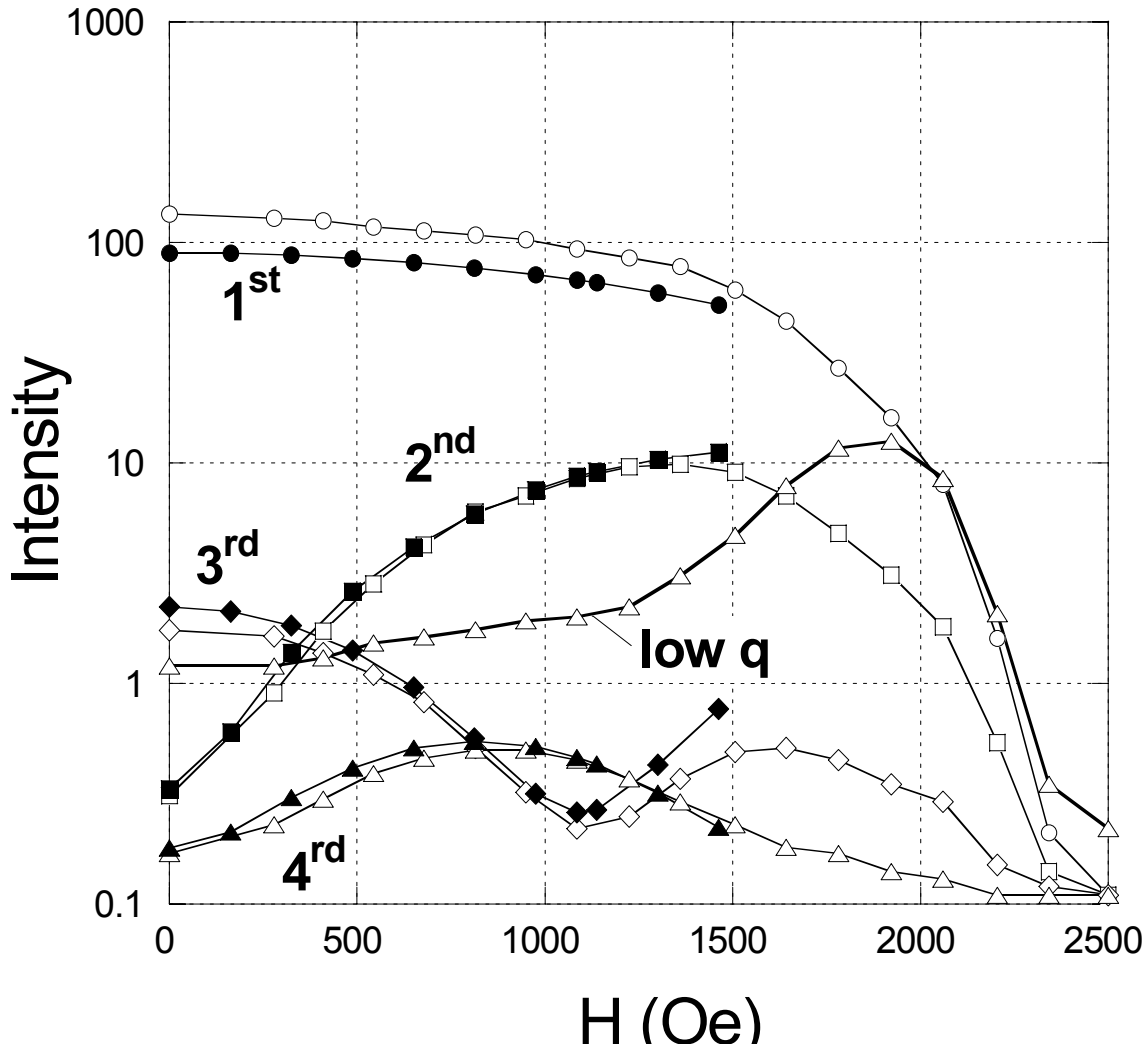

Figure 5: Scattering intensity of the different harmonics from the aligned domain pattern versus externally applied field. The open symbols are experimental data, while the solid symbols are theoretical fits to the data**.** The open diamonds show the scattering intensity development at very low q values, thus being a measure for the disorder in the system.

Figure 5